Materials Advances

ROYAL SOCIETY OF CHEMISTRY

PAPER

View Article Online
View Journal | View Issue

Cite this: *Mater. Adv.*, 2023, 4, 1656

Exploring the catalytic degradation of 4-nitrophenol and *in vitro* cytotoxicity of gold nanoparticle-doped NiAlTi LDH

Garima Rathee, †[a] Heerak Chugh,†[a] Sahil Kohli, [a] Rajesh K. Gaur[b] and Ramesh Chandra *[ac]

Nanoparticles have gained significant interest in both the diagnosis and therapeutic intervention of cancer. Here we describe a novel fabrication of gold-supported flower-like NiAlTi LDH by using a two-step process: first, a hydrothermal route for flower-like NiAlTi LDH synthesis and second, an ion-exchange and sodium borohydride reduction method for supporting gold over the NiAlTi LDH. The assembled Au@NiAlTi LDH nanomaterial was characterized by a variety of physicochemical techniques – XRD, FTIR, and TEM. The gold nanoparticles were found to be well supported over the surface of NiAlTi LDH, and were spherical and oval in shape with an average diameter ranging from 30 to 50 nm. Furthermore, we show the anticancer activity of the Au@NiAlTi LDH nanoparticles for the first time in human lung adenocarcinoma through an *in vitro* cytotoxicity assay. The cytotoxicity of Au@NiAlTi LDH is concentration-dependent, displaying an IC_{50} value of 441 μg ml^{-1}. We also tested the ability of the fabricated nano-hybrid in facilitating the catalytic degradation of 4-nitrophenol for wastewater remediation. The nanocatalyst was found to be an efficient agent for the catalytic degradation of 4-nitrophenol. The values of rate constant (k) and activation energy (E_a) were estimated as – 0.425 min^{-1} and 12.5 kJ mol^{-1}, respectively. The thermodynamic parameters (ΔH, ΔS and ΔG) indicate that the degradation of *p*-nitrophenol is an endothermic and spontaneous process. In addition, Au@NiAlTi LDH exhibits excellent reusability in the degradation of organic contaminants without a reportable performance falloff.

Received 13th December 2022,
Accepted 6th February 2023

DOI: 10.1039/d2ma01081j

rsc.li/materials-advances

1. Introduction

Layered double hydroxide (LDH) materials are a group of layer-structured inorganic compounds with water molecules, ions and metal cations within or between the layers.[1,2] LDHs are anionic clays with positively charged layers that are balanced by the intercalated negative counter-anions. The general formula of LDHs is $[M^{II}_{(1-x)}M^{III}_{x}(OH)_2]^{x+}(A^{n-})_{x/n}.mH_2O$, where M^{II} represents the divalent metal cations (Mg^{2+}, Ni^{2+}, *etc.*), M^{III} represents the trivalent metal cations (Fe^{3+}, Al^{3+}, Cr^{3+}, *etc.*), A^{n-} denotes the intercalated anions with negative charge n (Br^-, I^-, CO_3^{2-}, OH^-, *etc.*) and x designates the molar ratio between the cations ($M^{3+}/(M^{2+} + M^{3+})$). LDHs have attracted significant attention due to their remarkable potential in multiple scientific fields. These inorganic materials have shown numerous applications as catalysts, anion-exchangers, adsorbents, drug and catalyst carriers, electrode materials, and anticorrosion agents. These multi-utility materials have demonstrated low toxicity, high biocompatibility, eco-friendly synthesis and features, and acceptable loading efficiency. Due to this, LDH-based nanocomposites are considered as eco-friendly nanomaterials.[3–7]

Therapeutic application of gold and its complexes has gained significant attention because of their electrical and optical properties. Surface-enhanced emission, surface-plasmon resonance, and surface-enhanced Raman scattering are considered as some of the most promising alternative tools for catalysis, bio-sensing, bio-imaging, nano-based medicines, targeted drug delivery, and photothermal therapy.[8–11] Since gold nanoparticles (AuNPs) have a well-controlled size, high chemical stability, and surface functional properties, AuNPs and their hybrid materials are useful in biomedical research and as anti-cancer agents.[12] AuNPs and related materials have shown excellent applicability in numerous catalytic reactions, such as cross-coupling, photocatalysis, amination, nucleophilic

[a] *Drug Discovery & Development Laboratory, Department of Chemistry, University of Delhi, Delhi-110007, India. E-mail: rameshchandragroup@gmail.com*
[b] *Department of Medicine, University of Southern California, Los Angeles, CA 90033, USA*
[c] *Dr B. R. Ambedkar Centre for Biomedical Research, University of Delhi, Delhi-110007, India. E-mail: acbrdu@hotmail.com*
† Equal author contribution.

addition, sequential oxidative addition, oxidative C–C coupling, and benzylation of aromatics.[12–16] The support materials play a vital role in the stabilization of the AuNPs at different oxidation states, in monitoring the dispersion level and simultaneously acting as a buffer for electron transfer to the AuNPs.[13] Among the numerous available choices of materials having large surface areas, LDH is one of the most extensively used supports and has unique importance due to the intercalation properties.[17–19] The aforementioned features found only in LDH support materials make them an excellent choice for the fabrication of gold-supported nanocomposites. Lung cancer is one of the major causes of cancer-related deaths around the globe. Among the few types of lung cancers, non-small cell lung cancer (NSCLC) is more prevalent and accounts for approximately 80–85% of lung cancer cases.[20] Although there has been a worldwide effort to employ various conventional therapies such as invasive surgeries, non-invasive radiotherapy, and chemotherapy or different combinations of these to treat NSCLC, locally advanced and metastatic forms of the disease pose serious challenges. Additionally, toxicity, untargeted effects, and the development of resistance call for new innovative approaches.[21] The use of nanomaterials has surfaced as a non-invasive, targeted, safe, and multi-potent therapeutic in the fight against cancer.[22] Plentiful studies have reported the fabrication of drug/LDH nanohybrids by intercalating several pharmaceutical drugs such as camptothecin, methotrexate (MTX), fenbufen, diclofenac, *etc.*[17] Importantly, the functionalization of LDH materials with AuNPs might advance the biomedical applications of the LDH materials, and could be an ideal candidate for cancer treatment.

Industrialization in the developing world has resulted in tremendous water pollution due to several pollutants such as agricultural pesticides, and inorganic-, organic-, and bio-waste. Due to the rising anxieties regarding water pollution, wastewater treatment has become a topic of immediate priority. Unfortunately, the management of the contaminated sites and the disposal of the numerous organic compounds with the currently available techniques are inadequate. Organic pollutants such as antibiotics, nitroarenes, phenols, dyes, explosives, chlorophenols, and plastics are hazardous to the environment.[23–28] The disposal of untreated industrial wastewater is polluting aquatic systems and affecting all life forms dependent on these water bodies.[29] Application of current wastewater treatment strategies like multipurpose catalytic methods, homogeneous metal catalysts and metal complex catalysts may pose additional threats during wastewater treatment. For instance, in Fenton's oxidation, the iron-containing sludge could result in algae's proliferation, enzyme immobilization and genetic modification in bacteria.[30] To this end, numerous modifications have been introduced to purify wastewater. Noble metals (such as Au, Pd, Ni, and Pt) supported on LDH supports have emerged as promising candidates for numerous catalytic reactions.[31] Therefore, gold nanocomposites supported over an LDH support system could be a promising candidate for wastewater remediation due to the high chemical stability of Au-NPs.

We previously showed the impressive efficiency of ternary NiAlTi LDH in eliminating anionic dyes and antibiotics *via* an adsorption mechanism with an attained maximum adsorption capacity of 1250 mg g^{-1} for methyl orange, 2000 mg g^{-1} for orange II, and 238.09 mg g^{-1} for tetracycline.[6] We also described a methodology to support AuNPs over the surface of NiAlTi LDH in order to fabricate an efficient and reusable multipurpose nanocatalyst for several organic transformations.[31] This study provided a novel route for the synthesis of various biologically important xanthene, 1,4-dihydropyridine, polyhydroquinoline, and 4H-pyran derivatives.

Herein, we have designed flower-like NiAlTi LDH for the very first time and tested the utility of AuNPs supported on NiAlTi LDH as an anticancer agent by an *in vitro* cytotoxicity assay by using a human lung adenocarcinoma cell line. Additionally, we have tested the efficiency of the fabricated nano-hybrid in facilitating the catalytic degradation of organic pollutants for wastewater remediation.

2. Experimental section

2.1. Materials and methods

All the chemicals used for the fabrication of the nano-hybrid and for degradation studies were obtained from commercial sources and were used without further purification. The designed Au@NiAlTi LDH nano-hybrid was evaluated for its morphology and phase purity. The XRD patterns were obtained using an X-ray diffractometer (Model No. D8 DISCOVER). Morphological studies of the nanocomposite were evaluated on a TECNAI 200kV transmission electron microscopy system. The FTIR spectra were recorded on an IRAffinity-1S Fourier transform infrared spectrophotometer. The thermogravimetric analysis (TGA) was carried out using a LINSEIS L40/2052 system. A549 cells were obtained from NCCS, Pune and cultured in Dubecco's modified Eagle's medium (DMEM) (HiMedia) supplemented with 10% fetal bovine serum (HiMedia) and 1% antibiotic solution (HiMedia). Methylthiazolyldiphenyltetrazolium bromide (MTT) (Sigma Aldrich), a yellow tetrazole dye, was used for the MTT cytotoxicity assay.

2.2. Synthesis of NiAlTi LDH and Au@NiAlTi LDH

NiAlTi LDH was fabricated by making a few alterations in the previously reported hydrothermal method [1, 31]. In brief, a mixture of 2.74 g of $Ni(NO_3)_2{\cdot}6H_2O$, 1.77 g of $Al(NO_3)_3{\cdot}9H_2O$, 0.3 ml of $TiCl_4$, 1.5 g of urea, and 5 g of poly(vinylpyrrolidone) (PVP-10) was dissolved in distilled water, followed by aging for 48 hours in a hydrothermal autoclave at 130 °C. The material so-obtained was filtered, washed with deionized water and ethanol and dried at 60 °C. Gold was then supported on the NiAlTi LDH *via* an ion-exchange and $NaBH_4$ reduction method. First, 0.025 g of hydrogen tetrachloroaurate(III) hydrate was dissolved in 60 ml of water. Then, 600 mg of NiAlTi LDH was added to the gold solution and stirred for 12 hours. The sample was filtered, washed, and oven-dried at 60 °C. The desired material was added to 50 ml of toluene, followed by the

addition of a reducing agent ($NaBH_4$) and was stirred vigorously for 10 min. To this, 15 ml of ethanol was added and the mixture was stirred for the next 8 hours at room temperature. Finally, the Au@NiAlTi LDH nanocomposite was obtained by filtration and washing with deionized water and ethanol.

2.3. *In vitro* cytotoxicity assay

A549 lung adenocarcinoma cells were cultured in DMEM supplemented with 10% fetal bovine serum (FBS) and 1% antibiotics, penicillin and streptomycin (100 μg ml^{-1}). Cells were grown in 5% CO_2 in an air-humidified incubator at 37 °C. At ~80% confluency, the cells were harvested for the cytotoxicity assay essentially as described by the manufacturer with slight modifications. The cells were plated in a 96 well-plate at a density of 1×10^4 cells per well and incubated overnight. A 2 mg ml^{-1} stock solution of NiAlTi LDH and Au@NiAlTi LDH was prepared in distilled water. The solution was further diluted to a working concentration of 1 mg ml^{-1} with DMEM. The cells were treated with NiAlTi LDH or Au@NiAlTi at various concentrations ranging from 0 to 1000 μg ml^{-1} for 24 hours. Post-incubation, the effects of NiAlTi LDH and Au@NiAlTi LDH were evaluated using a freshly prepared methylthiazolyl-diphenyl-tetrazolium bromide (MTT) solution at a final concentration of 0.5 mg per ml per well. After 4 hours at 37 °C, the MTT solution was removed. Next, 100 μl of DMSO was added to each well to dissolve the formazan crystals and a reading was taken using a multi-plate reader at 570 nm.

2.4. Cell morphology assessment

Cell morphology was assessed using an inverted light microscope. A549 cells were seeded in a 6-well plate at a density of 5×10^3 cells per well. Cells were incubated at 37 °C with medium or various concentrations of Au@NiAlTi LDH (6.25 μg ml^{-1}, 31.25 μg ml^{-1}, 250 μg ml^{-1} and 1000 μg ml^{-1}) for 48 hours. After incubation, the medium was aspirated, and the cells were washed and suspended in 1× PBS for morphological assessment.

2.5. Catalytic degradation of 4-nitrophenol

The catalytic activity of Au@NiAlTi LDH was assessed by the degradation of 4-nitrophenol in the presence of $NaBH_4$. In a typical experiment, 2 ml of perfectly dispersed aqueous solution of Au@NiAlTi LDH (6 mg) was added to a mixture of 2 ml of 4-nitrophenol (0.05 M) and $NaBH_4$ (20 equivalent to 4-nitrophenol) at 30 °C. 10 μl of the reaction mixture was withdrawn at the indicated time, diluted with 3 ml of deionized water and swiftly filtered using a syringe filter. This diluted and filtered sample was analyzed by using UV-vis spectrometry. Initially, the amount of catalyst was optimized by varying the amount of Au@NiAlTi LDH. The reactions were also performed in the absence of $NaBH_4$ and the catalyst under identical reaction conditions. Experiments were also performed with NiAlTi LDH under similar conditions. Furthermore, a controlled set of experiments was performed by altering the temperature from 30 °C to 40° and then at 50 °C.

3. Results and discussion

3.1. Characterization of LDH and Au@LDH

The fabricated NiAlTi LDH and Au@NiAlTi LDH were characterized by using physicochemical methods such as XRD, FTIR, and TEM. The XRD patterns of NiAlTi LDH and Au@NiAlTi LDH are illustrated in Fig. 1(A). The XRD spectrum of the fabricated NiAlTi LDH illustrated in Fig. 1(A (a)) is in agreement with the previously reported spectrum of NiAlTi LDH.[6,31] The characteristic (00*L*) series ((003), (006) and (009)) are detected at 11.25, 22.70, and 39.34°, respectively, demonstrating the presence of the lamellar structure with carbonate ions and water molecules intercalated within the LDH layers. The acquired *d*-spacings for the (003) and (006) planes, 0.78 and 0.35 nm respectively, are similar to those of the reported Ti-integrated LDHs. The presence of (110) planes positioned at 25.28° confirms the existence of the TiO_2 anatase plane. Additionally, the XRD spectrum of Au@NiAlTi LDH was found to be similar to that of the NiAlTi LDH spectrum. Fig. 1(A (b)) illustrates the XRD spectrum of Au@NiAlTi LDH. The obtained spectrum confirms the existence of gold nanoparticles. The recorded spectrum embraced the characteristic peaks of NiAlTi LDH along with two distinct diffraction peaks at 38.1° and 45.2°, confirming the existence of gold nanoparticles. These two diffraction peaks, located at 38.1° and 45.2°, which are different from the diffraction peaks of NiAlTi LDH could be attributed to the standard Braggs reflection planes ((111) and (200), respectively) of the gold nanoparticles. These peaks confirm the successful supporting of gold nanoparticles over the surface of NiAlTi LDH to fabricate Au@NiAlTi LDH.

Fig. 1(B) illustrates the Fourier-transform infrared (FTIR) spectra of (a) NiAlTi LDH and (b) Au@NiAlTi LDH. The obtained FTIR spectra were found to be in great correlation with the previously reported data.[6,31] Fig. 1(B (a)) presents the FTIR spectrum of NiAlTi LDH comprised of a broad band positioned at 3387 cm^{-1} approving the existence of the hydroxyl groups of the brucite layers along with interlayered water molecules. The presence of the hydrogen-bonding among the water molecules and carbonate ions could be confirmed by the

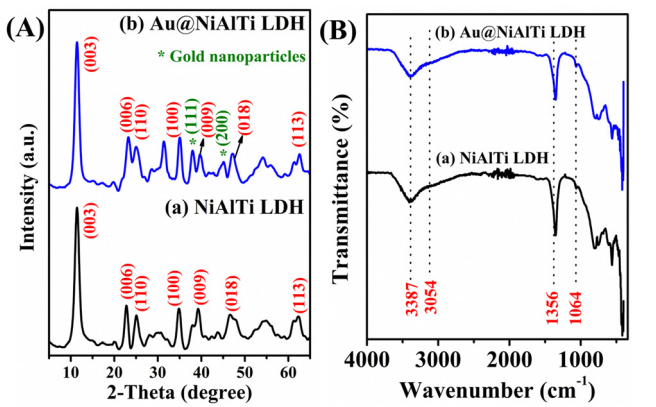

Fig. 1 (A) The XRD spectra of (a) NiAlTi LDH and (b) Au@NiAlTi LDH; (B) the FTIR spectra of (a) NiAlTi LDH and (b) Au@NiAlTi LDH.

occurrence of a shoulder band located at 3054 cm^{-1}. Moreover, the presence of the carbonate ions within the interlayers could be confirmed by the existence of an asymmetric band situated at 1356 cm^{-1}. On supporting the gold nanoparticles over the surface of the NiAlTi LDH, no significant change in the FTIR spectrum was observed, as depicted in Fig. 1(B (b)).

Fig. 2 depicts the high-resolution transmission electron microscopy (HRTEM) images of Au@NiAlTi LDH at different resolutions. The HRTEM images confirm the support of the gold nanoparticles over the surface of NiAlTi LDH. Fig. 2(a) represents the gold nanoparticles. Most of the gold nanoparticles are either spherical or oval in shape with a diameter within the range of 30–50 nm. Fig. 2(b) represents gold nanoparticles supported over the surface of NiAlTi LDH. The illustrated nanoparticles are oval in shape. Fig. 2(d) confirms the formation of fringes with d-spacing as 0.81 and 0.36 nm. Fig. 2(e) and (f) depict the flower-like morphology of NiAlTi LDH.

3.2. Evaluation of the cytotoxic effect of the nanoparticles using the MTT assay

A variety of cell-based assays are available to evaluate the anticancer activity of drug molecules. The MTT assay is one of the simplest and most widely used assays to determine the drug response *in vitro*. MTT is a colorimetric assay, which estimates cell proliferation in correlation to the mitochondrial activity. In live cells, NADPH-dependent oxidoreductase activity reduces the tetrazolium salt to formazan crystals, which can be estimated spectrophotometrically. Thus, the degree of cytotoxicity of a test compound will be proportional to the amount of formazan produced; more NADPH molecules in a cell will produce more crystals.

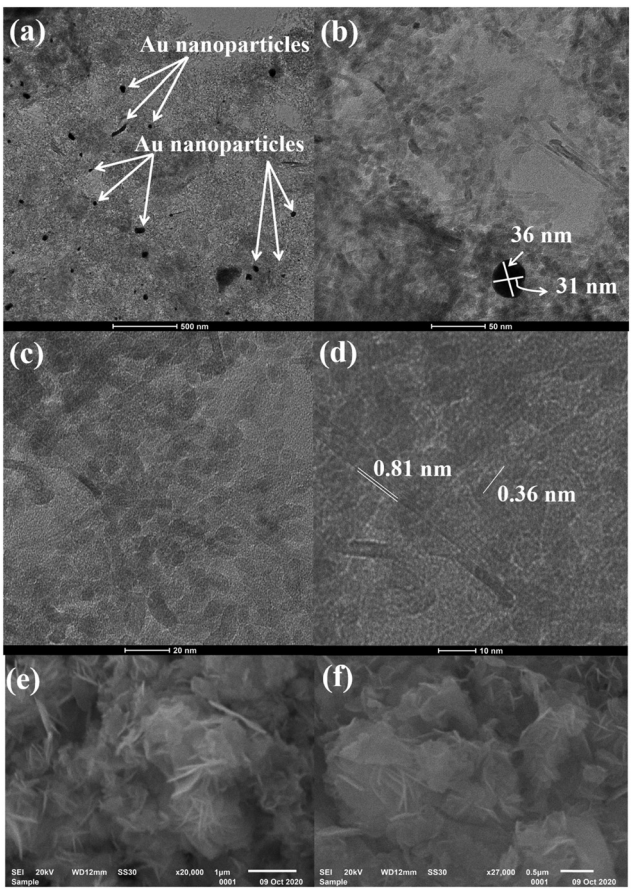

Fig. 2 The HRTEM images of Au@NiAlTi LDH at different resolutions (a) 500 nm, (b) 50 nm, (c) 20 nm and (d) 10 nm. The SEM images depicting the flower-like morphology of NiAlTi LDH at different resolutions (e) and (f).

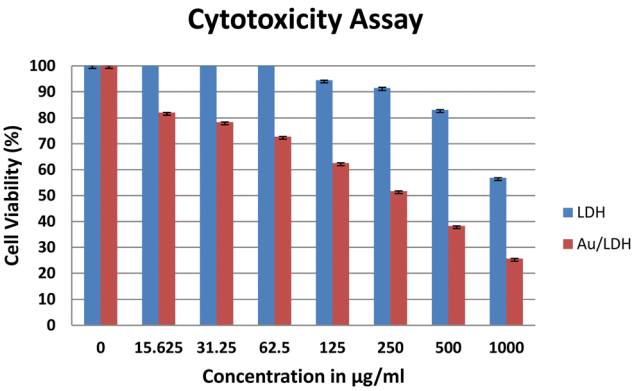

Fig. 3 The MTT assay to assess the cytotoxicity of NiAlTi LDH (blue) and Au@NiAlTi LDH (red) against A549 lung adenocarcinoma cells.

We employed lung cancer as a model to evaluate the anticancer activity of the synthesized, fabricated material. To determine whether or not the nanoparticles could kill the cancer cells, lung adenocarcinoma cells (A549) were treated in triplicate with NiAlTi LDH and Au@NiAlTi LDH for 24 hours at 37 °C. The concentration range was 15.6, 31.3, 62.5, 125, 250, 500, and 1000 µg ml^{-1}. After treatment, the cells were incubated with MTT. As shown in Fig. 3, the effects of both NiAlTi LDH and Au@NiAlTi LDH are concentration-dependent. Importantly, Au@NiAlTi LDH showed significantly stronger cytotoxicity as compared to NiAlTi LDH (Fig. 3). The IC_{50} values for Au@NiAlTi LDH and NiAlTi were calculated to be 441 µg ml^{-1} and 1185.75 µg ml^{-1}, respectively.

3.3. Cell morphology assessment

A549 non-small cell lung cancer cells were treated with different concentrations – 0 µg ml^{-1}, 6.25 µg ml^{-1}, 31.25 µg ml^{-1}, 250 µg ml^{-1} and 1000 µg ml^{-1} of Au@NiAlTi LDH for 48 hours. The inverted microscopic images showed that the Au@NiAlTi LDH altered the morphology of A549 cells in a concentration-dependent manner compared to the control. The treatment showed cell shrinkage, loss of epithelial characteristics and cell detachment, suggestive of cell death with increasing concentrations of Au@NiAlTi LDH (Fig. 4). Thus, the above-mentioned morphological changes and reduced cell proliferation validated by MTT assay establish a potential anti-cancer effect of Au@NiAlTi LDH.

3.4. Catalytic degradation of 4-nitrophenol

The utility of Au@NiAlTi LDH was also explored for the hydrogenation of toxic *p*-nitrophenol into a less toxic product (*p*-aminophenol) in the presence of an excess of $NaBH_4$ by using UV-

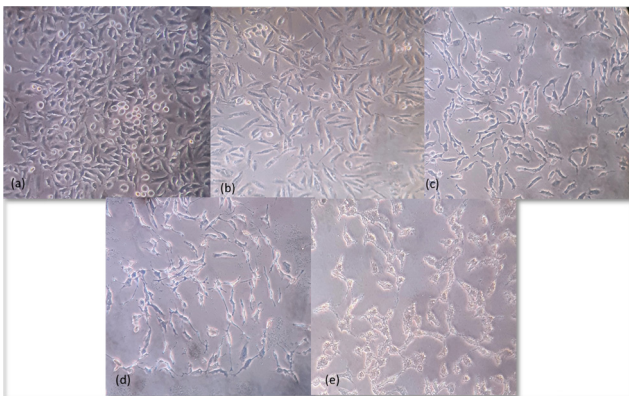

Fig. 4 The inverted light microscopy images of cells: A549 cells were untreated (a) 0 μg ml^{-1} or treated with increasing concentrations of Au@NiAlTi LDH; (b) 6.25 μg ml^{-1}; (c) 31.25 μg ml^{-1}; (d) 250 μg ml^{-1} and (e) 1000 μg ml^{-1}.

vis absorption spectra. In the absence of $NaBH_4$, *p*-nitrophenol gives its characteristic peak at 313 nm whereas with the addition of $NaBH_4$, the *p*-nitrophenol gets converted into *p*-nitrophenoxide ions that display a characteristic peak at 400 nm. One other distinct peak that appears during the degradation of 4-nitrophenol is that at 300 nm belonging to *p*-aminophenol.

During the degradation process, the intensity of the characteristic peak of *p*-nitrophenol gradually decreased, while a new peak of *p*-aminophenol came into existence with increasing time at 300 nm. Additionally, the colour change after the completion of the degradation process was very prominent, from yellow to colourless, as depicted in Fig. 5(h). Initially, the catalyst amount was optimized and 6 mg of the catalyst was selected as the optimum amount for the degradation process (illustrated in Fig. 5(a and b)). Catalytic degradation increased with increasing amount of catalyst. With 6 mg of Au@NiAlTi LDH, 4-nitrophenol was completely hydrogenated (100%) to *p*-aminophenol within 12 minutes of the reaction time. Furthermore, the reaction kinetics were evaluated by using a pseudo-first order kinetic equation as excess amount of $NaBH_4$ was used (20 equivalent to 4-nitrophenol). The pseudo-first order kinetic equation is described as:

$$-\ln(a_t/a_0) = kt \quad (1)$$

where, 'a_0' and 'a_t' represent the respective absorbance values at time = 0 and t, respectively, 'k' represents the rate constant and t denotes the time of the reaction. On plotting $\ln(a_t/a_0)$ *vs.* k, a straight line is observed. From the slope of the obtained

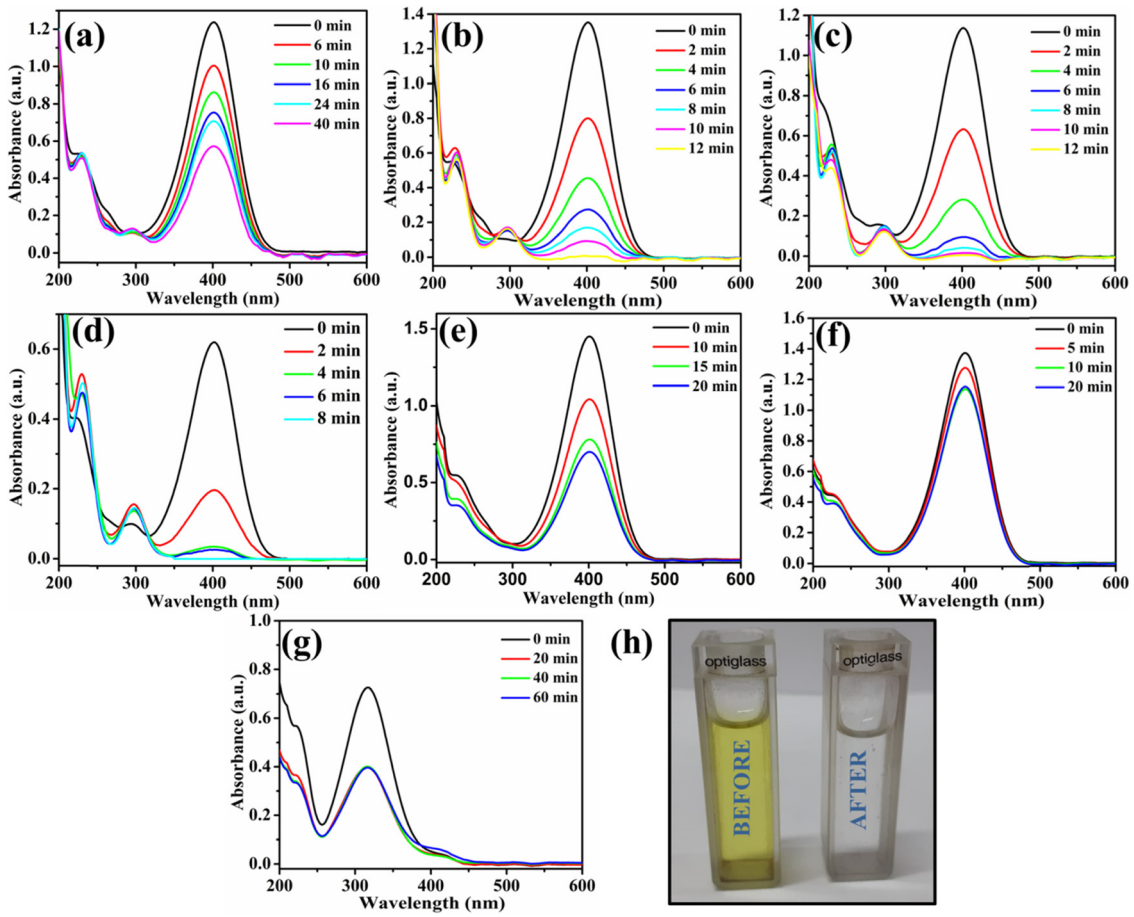

Fig. 5 The UV-vis absorption spectra of catalytic degradation of *p*-nitrophenol (a) with 4 mg of Au@NiAlTi LDH at 30 °C, (b) with 6 mg of Au@NiAlTi LDH at 30 °C, (c) with 6 mg of Au@NiAlTi LDH at 40 °C, (d) with 6 mg of Au@NiAlTi LDH at 50 °C, (e) with 6 mg of NiAlTi LDH at 30 °C, (f) in the absence of Au@NiAlTi LDH and (g) in the absence of $NaBH_4$, and (h) an image presenting the color change after complete degradation of *p*-nitrophenol.

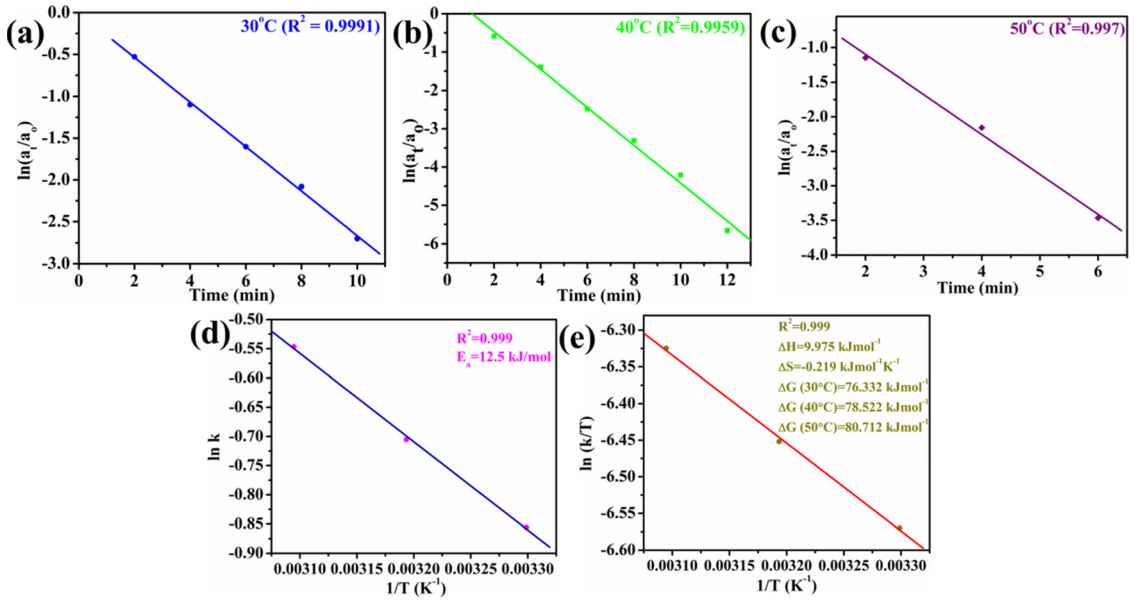

Fig. 6 Plots of (a) $\ln(a_t/a_o)$ *vs.* time (min) at 30 °C, (b) $\ln(a_t/a_o)$ *vs.* time (min) at 40 °C, (c) $\ln(a_t/a_o)$ *vs.* time (min) at 50 °C, (d) ln *k* *vs.* $1/T$ (K^{-1}), and (e) ln (k/T) *vs.* $1/T$.

straight line, the rate constant (k) is obtained as 0.425 min^{-1} with correlation coefficient approximately equal to 1 (illustrated in Fig. 6(a)).

Moreover, the influence of the temperature on the catalytic activity of Au@NiAlTi LDH was also investigated by performing the degradation at 40 °C and 50 °C, as depicted in Fig. 5(c) and (d), respectively. With a rise in temperature, the rate constant also got enhanced, from 0.425 (at 30 °C) to 0.494 (at 40 °C) and further to 0.579 min^{-1} (at 50 °C). From the obtained thermodynamic data, various other thermodynamic parameters such as E_a, ΔH, ΔS, and ΔG are also calculated by using the thermodynamics equations listed below (eqn (2)–(4)).

$$\ln k = \ln A - E_a/RT \quad (2)$$

$$\ln(k/T) = \ln(K/h) - \Delta H/RT + \Delta S/R \quad (3)$$

$$\Delta G = \Delta H - T\Delta S \quad (4)$$

where, 'k' represents the rate constant, 'A' represents the Arrhenius factor, 'T' symbolizes the temperature in kelvin, 'R' is the gas constant, 'E_a' signifies the activation energy, 'K' represents the Boltzmann constant, 'h' denotes the Planck constant, and ΔH, ΔS and ΔG symbolize the enthalpy, entropy and Gibbs free energy of the system, respectively. Eqn (2), which is the Arrhenius equation, was used for the calculation of the activation energy, from the slope obtained from the linearly fitted plot between ln k *vs.* ($1/T$), represented in Fig. 6(d). The activated energy (E_a) for the catalytic hydrogenation of 4-nitrophenol by Au@NiAlTi LDH was estimated as 12.5 kJ mol^{-1}. By employing eqn (3), ΔH and ΔS were evaluated from the slope and intercept of the linearly fitted plot between ln (k/T) and $1/T$ (Fig. 5(e)). The values of ΔH, and ΔS were calculated as 9.975 kJ mol^{-1} and −0.219 kJ mol^{-1} K^{-1}, respectively. Furthermore, by using eqn (4) and the values of ΔH and ΔS, the Gibbs free energy was calculated at 303, 313, and 323 K. The values of ΔG at 303, 313, and 323 K were found to be 76.332, 78.522, and 80.712 kJ mol^{-1}. All the obtained values are summarized in Table 1. From the obtained thermodynamic parameters, it could be claimed that the catalytic degradation of *p*-nitrophenol by Au@NiAlTi LDH is an endothermic and non-spontaneous process.

Additionally, we have also performed the catalytic degradation of 4-nitrophenol by using simple NiAlTi LDH as the catalyst, as illustrated in Fig. 5(e). The obtained adsorption spectra exhibited decline in the characteristic peak of 4-nitrophenoxide ions at 400 nm; however, no new peak of 4-nitroaniline was observed at 300 nm. From the obtained results, it could be inferred that due to high adsorption capacity executed by NiAlTi LDH, in this case, instead of catalytic degradation of 4-nitrophenol, the adsorption of the *p*-nitrophenoxide ions takes place within the layers of NiAlTi LDH by replacing the carbonate ions and water molecules present within the interlayers of the NiAlTi LDH moiety. Such observations are reported due to the absence of gold nanoparticles over the surface of NiAlTi LDH. Moreover, the control experiments were also performed in the absence of Au@NiAlTi LDH and in the absence of $NaBH_4$ (Fig. 5(f) and (g)). From the obtained data, it could be concluded that the reaction did not proceed significantly in either of the cases.

To achieve understanding of the reaction pathway of Au@NiAlTi LDH for catalytic degradation of 4-NP, a tentative

Table 1 Estimated thermodynamic parameters

Temp. (K)	k (min^{-1})	ΔG (kJ mol^{-1})	E_a (kJ mol^{-1})	ΔH (kJ mol^{-1})	ΔS (kJ mol^{-1} K^{-1})
303	0.425	76.332	12.5	9.975	−0.219
313	0.494	78.522			
323	0.579	80.712			

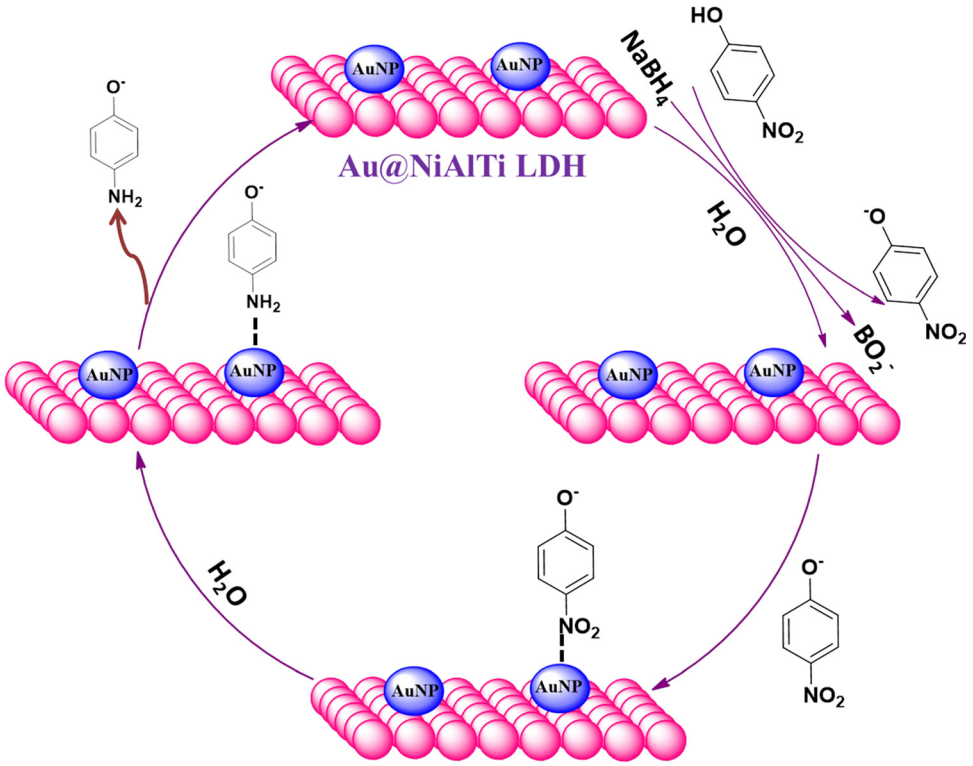

Fig. 7 Possible mechanism for Au@NiAlTi LDH catalyzed degradation of 4-nitrophenol.

mechanism based on the theoretical aspects has been introduced in Fig. 7. Initially, when $NaBH_4$ is added to the aqueous solution of 4-nitrophenol, 4-nitrophenol is converted into 4-nitrophenoxide ions, along with BH_4^- and active hydrogen species present in the solution. The reactants and reagents get adsorbed over the surface of the catalyst. A very vital role is played by the gold nanoparticles supported over the surface of the NiAlTi LDH in Au@NiAlTi LDH by transmitting the active hydrogen species produced by BH_4^- to 4-nitrophenoxide ions, resulting into the activation of the hydrogenation process of 4-nitrophenol into 4-aminophenol. Finally, 4-aminophenol is desorbed from the catalytic surface and furthermore the catalytic cycle continues for another 4-nitrophenol molecules.

Finally, one of the most important characteristics of a catalyst, *i.e.* reusability, was estimated. For reusability, the catalyst was filtered after the completion of the reaction and washed repetitively first with water and then with methanol and further vacuum-treated at room temperature. When the catalyst was dried completely it was used for the next degradation cycle and the same procedure was repeated again. From the obtained results, no significant loss in the catalytic efficiency of the Au@NiAlTi LDH was observed up to 5 cycles. In each case, complete degradation was obtained. The introduced Au@NiAlTi LDH was also compared with the previously reported nanocatalysts (Table 2).[32–36] On comparison with other previously reported catalysts, it can be stated that Au@NiAlTi LDH showed greater catalytic degradation of 4-NP.

4. Conclusion

We have successfully introduced the fabrication of gold-supported NiAlTi LDH by using a two-step process: the first being a hydrothermal route for NiAlTi LDH synthesis and the second involving an ion-exchange and sodium borohydride reduction method for gold support over the NiAlTi LDH. The gold nanoparticles were supported successfully over the surface of the NiAlTi LDH and most of the gold nanoparticles are either spherical or oval in shape with a diameter within the range of 30–50 nm. The nanomaterial obtained by supporting gold

Table 2 Comparative study of the catalytic efficiency of Au@NiAlTi LDH with other reported catalysts

Entry	Catalyst	Pollutant	Reaction time	k	Degradation (%)
1	PTSC/AuNPs[36]	4-NP	6 h	1.6×10^{-4} s^{-1}	80
2	Fe_3O_4@SiO_2@CeO_2/Au-Pd spheres[33]	4-NP	12 min	1.53×10^{-3}	95.1
3	Au NPs[34]	4-NP	120 min	2.67×10^{-3} min^{-1}	—
4	Ag_2O–ZnO composite nanocones[35]	4-NP	60 min	0.0636 min^{-1}	99
5	Au@NiAlTi LDH	4-NP	12 min	0.425 min^{-1}	Present study

nanoparticles over the surface of NiAlTi LDH was efficiently used for multiple applications. The *in vitro* cytotoxicity assay results evidenced that the effects of both NiAlTi LDH and Au@NiAlTi LDH are concentration-dependent. Moreover, Au@NiAlTi LDH showed a better cytotoxic effect against cancer cells than NiAlTi LDH. The IC_{50} value for Au@NiAlTi LDH was estimated to be 441 μg ml^{-1}. Additionally, the efficiency of the fabricated nano-hybrid in facilitating the catalytic degradation of 4-nitrophenol for wastewater remediation was also evaluated. The nano-catalyst was found to be an efficient agent for the catalytic degradation of 4-nitrophenol. The rate constant and activation energy (E_a) were estimated as 0.425 min^{-1} and 12.5 kJ mol^{-1}, respectively. Other thermodynamic parameters such as ΔH, ΔS and ΔG were also calculated for the degradation of *p*-nitrophenol. From the obtained results, the catalytic degradation of *p*-nitrophenol was found to be an endothermic and spontaneous process. Besides, Au@NiAlTi LDH exhibited excellent reusability in the degradation of organic contaminants without reportable performance falloff. Thus, this study has established the groundwork of two potential applications of the newly fabricated Au@NiAlTi LDH in cancer therapeutics and wastewater remediation.

Author contributions

G. R. and H. C. contributed equally to the manuscript as equal first authors. G. R. and R. C. designed the schemes. G. R. and S. K. synthesized the materials and evaluated the degradation of 4-nitrophenol. H. C. performed the biological study. G. R. and H. C. evaluated the data and prepared the figures and tables. G. R., H. C. and R. C. revised and reviewed the manuscript.

Conflicts of interest

The authors declare no conflicts of interest.

Acknowledgements

The authors are grateful to the Science and Engineering Research Board (SERB) (DST No. EMR/2016/002976) for providing funding to Prof. Ramesh Chandra and are also thankful to the University of Delhi, Delhi, India-110007.

References

1 L. Mohapatra and K. Parida, *J. Mater. Chem. A*, 2016, 4.
2 X. Jin, Y. Koizumi, K. Yamaguchi, K. Nozaki and N. Mizuno, *J. Am. Chem. Soc.*, 2017, **139**, 13821–13829.
3 G. Rathee, S. Kohli, N. Singh, A. Awasthi and R. Chandra, *ACS Omega*, 2020, **5**, 15673–15680.
4 G. Rathee, A. Awasthi, D. Sood, R. Tomar, V. Tomar and R. Chandra, *Sci. Rep.*, 2018, **24**, 35–39.
5 G. Rathee, S. Kohli, A. Awasthi, N. Singh and R. Chandra, *RSC Adv.*, 2020, **10**, 19371–19381.
6 G. Rathee, N. Singh and R. Chandra, *ACS Omega*, 2020, **5**, 2368–2377.
7 Z. Zhang, Z. Hua, J. Lang, Y. Song, Q. Zhang, Q. Han, H. Fan, M. Gao, X. Li and J. Yang, *CrystEngComm*, 2019, **21**, 4607–4619.
8 A. Wicki, D. Witzigmann, V. Balasubramanian and J. Huwyler, *J. Control. Release*, 2015, 200.
9 X. Huang and M. A. El-Sayed, *J. Adv. Res.*, 2010, 1.
10 S. Rajeshkumar, *J. Genet. Eng. Biotechnol.*, 2016, **14**, 195–202.
11 G. K. Ahirwal and C. K. Mitra, *Sensors*, 2011, **1**, 232–237.
12 Q. Yu, J. Li, Y. Zhang, Y. Wang, L. Liu and M. Li, *Sci. Rep.*, 2011, **1**, 232–237.
13 G. Mikami, F. Grosu, S. Kawamura, Y. Yoshida, G. Carja and Y. Izumi, *Appl. Catal., B*, 2016, **199**, 260–271.
14 F. Zhang, X. Zhao, C. Feng, B. Li, T. Chen, W. Lu, X. Lei and S. Xu, *ACS Catal.*, 2011, **1**, 232–237.
15 J. Gong, *Chem. Rev.*, 2012, 112.
16 C. G. Silva, Y. Bouizi, V. Fornés and H. García, *J. Am. Chem. Soc.*, 2009, **131**, 13833–13839.
17 X. Q. Zhang, M. G. Zeng, S. P. Li and X. D. Li, *Colloids Surf., B*, 2014, **117**, 98–106.
18 X. Li, X. Hao, Z. Wang, A. Abudula and G. Guan, *J. Power Sources*, 2017, **347**, 193–200.
19 H. Wang, T. Zhou, P. Li, Z. Cao, W. Xi, Y. Zhao and Y. Ding, *ACS Sustainable Chem. Eng.*, 2018, **6**, 380–388.
20 J. R. Molina, P. Yang, S. D. Cassivi, S. E. Schild and A. A. Adjei, *Mayo Clin. Proc.*, 2008, **83**, 584–594.
21 H. Chugh, D. Sood, I. Chandra, V. Tomar, G. Dhawan and R. Chandra, *Artif. Cells, Nanomed., Biotechnol.*, 2018, 46.
22 S. Hussain, *Adv. Exp. Med. Biol.*, 2016, **890**, 137–147.
23 R. L. Wang, D. P. Li, L. J. Wang, X. Zhang, Z. Y. Zhou, J. L. Mu and Z. M. Su, *Dalton Trans.*, 2019, **48**, 1051–1059.
24 P. P. Ghimire, L. Zhang, U. A. Kinga, Q. Guo, B. Jiang and M. Jaroniec, *J. Mater. Chem. A*, 2019, **7**, 9618–9628.
25 R. Abazari, A. R. Mahjoub and J. Shariati, *J. Hazard. Mater.*, 2019, **366**, 439–451.
26 D. Chen, X. Zhu, J. Huang, G. Wang, Y. Zhao, F. Chen, J. Wei, Z. Song and Y. Zhao, *Anal. Chem.*, 2018, **90**, 9048–9054.
27 C. A. Choy, B. H. Robison, T. O. Gagne, B. Erwin, E. Firl, R. U. Halden, J. A. Hamilton, K. Katija, S. E. Lisin, C. Rolsky and K. S. Van Houtan, *Sci. Rep.*, 2019, **9**, 7843.
28 M. D'Alessandro, V. Esposito, E. M. D. Porporato, D. Berto, M. Renzi, S. Giacobbe, G. Scotti, P. Consoli, G. Valastro, F. Andaloro and T. Romeo, *Environ. Pollut.*, 2018, **242**, 1546–1556.
29 H. Hartikainen, *J. Trace Elem. Med. Biol.*, 2005, **18**, 309–318.
30 A. Chanda, S. K. Khetan, D. Banerjee, A. Ghosh and T. J. Collins, *J. Am. Chem. Soc.*, 2006, **128**, 12058–12059.
31 G. Rathee, S. Kohli, S. Panchal, N. Singh, A. Awasthi, S. Singh, A. Singh, S. Hooda and R. Chandra, *ACS Omega*, 2020, **5**, 23967–23974.
32 J. Luo, N. Zhang, R. Liu and X. Liu, *RSC Adv.*, 2014, **4**, 64816–64824.
33 N. Li, F. Zhang, H. Wang and S. Hou, *Eng. Sci.*, 2019, **7**, 72–79.
34 K. B. Narayanan and N. Sakthivel, *J. Hazard. Mater.*, 2011, **189**, 519–525.
35 U. Chakraborty, G. Bhanjana, Kannu, N. Kaur, R. Sharma, G. Kaur, A. Kaushik and G. R. Chaudhary, *J. Hazard. Mater.*, 2021, **416**, 125771.
36 L. F. Villalobos, P. Neelakanda, M. Karunakaran, D. Cha and K. V. Peinemann, *Catal. Today*, 2014, **236**, 92–97.